Langmuir Article

pubs.acs.org/Langmuir

Macroscopic Ordering of Polystyrene Carboxylate-Modified Nanospheres Self-Assembled at the Water−Air Interface

Evgeny Sirotkin,* Julius D. Apweiler, and Feodor Y. Ogrin

School of Physics, University of Exeter, Exeter, EX4 4QL U.K.

Received March 9, 2010. Revised Manuscript Received April 6, 2010

We present results from an experimental study of ordering characteristics in monolayers of polystyrene nanospheres self-assembled at a water−air interface. We demonstrate that the interaction of spheres, governed by the dissemination of surface charge, leads to the formation of macroscopic close-packed ordered areas or "domains" with a well-defined orientation of the lattice axes over areas of 25 mm^2. It was found that by changing the surface chemistry of the spheres it is possible to modify the balance between the attractive and repulsive forces and thus to control the ordering characteristics. We implemented a model that simulates the process of self-assembly and examines the ordering characteristics for layers with different ratio between attractive and repulsive forces. A good qualitative agreement was found between the simulations and experiment. These studies are technologically relevant as a method of producing nanosphere templates for large area patterned materials.

1. Introduction

Ordered colloidal systems obtained via the method of nanosphere self-assembly play an important role in a wide range of applications such as photonic materials,[1,2] high-density magnetic data storage,[3,4] biosensors,[5] and preparation of materials with micro- and nanometer scale patterns. Colloids can be easily manipulated, thus giving numerous possibilities for controlling the processes of assembly. Micropatterned colloidal assemblies can be produced with lithographically patterned electrodes,[5,10] micromolds,[11] electric-field-induced assembly,[12,13] variable current density on electrode substrate,[13,15] magnetic field,[16] patterned substrates,[17] and the method of electrophoretic assembly.[14,18] Many of these experimental methods are employed to produce arrays of submicrometer particles. The focus is generally on the order parameter which has direct relation to the average size of domains (highly ordered regions with well-defined orientation of principal axes). The structural rearrangements and observations of order−disorder transitions in colloidal systems have been reported in a number of theoretical and experimental works on ionic colloidal dispersions/suspensions.[19−28] Far less attention though has been given to the study of monolayers of colloid spheres.[16,35−41] Yet, the latter are technologically very important as templates for large-area patterning applications.[6−9] As has been shown in one of the original studies of 2D colloid systems,[29] the charge-stabilized colloidal polystyrene spheres can be trapped at the air−water interface and organized in a crystal-like structure forming a 2D hexagonal lattice. Such behavior was attributed to stabilization due to the dipole−dipole repulsive interactions for which theoretical treatments of the phenomenon have subsequently been given.[30−33] Some experiments on reentrant ordering rearrangements by varying the particle charge density have already been shown on ionic colloidal dispersions of polystyrene and latex spheres.[20−22,27,28] It has been demonstrated that the interaction forces are responsible for structural ordering in colloidal dispersions. At a particular ionic strength they exhibit spatial ordering over distances considerably greater than the particle diameter as a result of long-ranged electrostatic repulsion forces. Later, it was shown that for 2D colloidal systems governed by

*Corresponding author. E-mail: E.Sirotkin@exeter.ac.uk.

(1) Lin, S. Y.; Chow, E.; Hietala, V.; Villeneuve, P. R.; Joannopoulos, J. D. *Science* **1998**, *282*, 274–276.
(2) Painter, O.; et al. *Science* **1999**, *284*, 1819–1821.
(3) Haginoya, C.; Ishibashi, M.; Koike, K. *Appl. Phys. Lett.* **1997**, *71*, 2934–2936.
(4) Weekes, S. M.; Ogrin, F. Y.; Murray, W. A. *Langmuir* **2004**, *20*, 11208–11212.
(5) Velev, O. D.; Kaler, E. W. *Langmuir* **1999**, *15*, 3693–3698.
(6) Li, S. P.; Lew, W. S.; Xu, Y. B. *Appl. Phys. Lett.* **2000**, *76*, 748.
(7) Haynes, C. L.; Van Duyne, R. P. *J. Phys. Chem. B* **2001**, *105*, 5599.
(8) Goncharov, A.; et al. *J. Magn. Magn. Mater.* **2005**, *286*, 1–4.
(9) Albrecht, M.; et al. *Nat. Mater.* **2005**, *4*, 203.
(10) Yeh, S. R.; Seul, M.; Shraiman, B. I. *Nature* **1997**, *386*, 57–59.
(11) Kim, E.; Xia, Y. N.; Whitesides, G. M. *Adv. Mater.* **1996**, *8*, 245–247.
(12) Yi, G. R.; Moon, J. H.; Yang, S. M. *Adv. Mater.* **2001**, *13*, 1185.
(13) Trau, M.; Saville, D. A.; Aksay, I. A. *Science* **1996**, *272*, 706–709.
(14) Bohmer, M. *Langmuir* **1996**, *12*, 5747–5750.
(15) Trau, M.; Saville, D. A.; Aksay, I. A. *Langmuir* **1997**, *13*, 6375–6381.
(16) Miao, Y. H.; Geng, D. L.; Helseth, L. E. *Langmuir* **2006**, *13*, 5572–5574.
(17) Ye, Y. H.; Badilescu, S.; Truong, V. V.; et al. *Appl. Phys. Lett.* **2001**, *79*, 872–874.
(18) Hayward, R. C.; Saville, D. A.; Aksay, I. A. *Nature* **2000**, *404*, 56–59.
(19) Yoshida, H.; et al. *Langmuir* **1999**, *15*, 2684–2702.
(20) Toyotama, A.; et al. *Langmuir* **2003**, *19*, 3236–3239.
(21) Yamanaka, J.; et al. *Langmuir* **1999**, *15*, 4198–4202.
(22) Yamanaka, J.; et al. *Phys. Rev. Lett.* **1998**, *80*, 5806–5809.
(23) Kaneko, T.; et al. *Langmuir* **2005**, *21*, 9698–9703.
(24) Mohanty, P. S.; et al. *Langmuir* **2005**, *21*, 11678–11683.
(25) Okubo, T. *Langmuir* **1994**, *10*, 1695–1702.
(26) Quesada-Perez, M.; Callejas-Fernandez, J.; Hidalgo-Alvarez, R. *Adv. Colloid Interface Sci.* **2002**, *95*, 295–315.
(27) Russel, W. B. *Nature* **2003**, *421*, 490–491.
(28) Yethiraj, A.; van Blaaderen, A. *Nature* **2003**, *421*, 6922, 513−517
(29) Pieranski, P. *Phys. Rev. Lett.* **1980**, *45*, 569–572.
(30) Hurd, A. J. *J. Phys. A* **1985**, *18*, 1055–1060.
(31) Earnshaw, J. C. *J. Phys. D: Appl. Phys.* **1986**, *19*, 1863–1868.
(32) Nikolaides, M. G.; et al. *Nature* **2002**, *420*, 299–301.
(33) Dominguez, A.; Oettel, M. *J. Chem. Phys.* **2008**, *128*, 114904.
(34) Weekes, S. M.; Ogrin, F. Y.; Murray, W. A.; Keatley, P. S. *Langmuir* **2007**, *23*, 1057–1060.
(35) Terao, T.; Nakayama, T. *Phys. Rev. E* **1999**, *60*, 7157–7162.
(36) Onoda, G. Y. *Phys. Rev. Lett.* **1985**, *55*, 226–229.
(37) Ruiz-Garca, J.; Gamez-Corrales, R.; Ivlev, B. I. *Phys. Rev. E* **1998**, *58*, 660–663.
(38) Gomez-Guzman, O.; Ruiz-Garcia, J. *J. Colloid Interface Sci.* **2005**, *291*, 1–6.
(39) Horozov, T. S.; et al. *Langmuir* **2003**, *19*, 2822–2829.
(40) Ghezzi, F.; Earnshaw, J. C.; Finnis, M.; McCluney, M. *J. Colloid Interface Sci.* **2001**, *238*, 433–446.
(41) Aveyard, R.; Clint, J. H.; Nees, D.; Paunov, V. N. *Langmuir* **2000**, *16*, 1969–1979.

repulsive dipolar forces a more ordered system can be observed when the interaction strength between the particles is increased.[16]

In this article we are investigating the ability to control the ordering in the colloidal monolayers self-assembled at the water−air interface. We report on observations of macroscopic ordering of polystyrene nanospheres of two different sizes. We show that by changing the electrostatic environment of the water−air interface, we can modify the average domain size of the lattice. On the basis of the result of simulations, we suggest that the size of the ordered domains and the overall correlation of spheres in the monolayer can be modified via tuning the repulsion−attraction balance between spheres. It is shown that by changing the pH factor of water the system can go from a disordered state to an ordered state. It is also predicted that there should be a well-defined state that corresponds to an energy minimum for which the order parameter is maximal. From simulations we can observe that the system changes from a disordered state to a more ordered state and then back by increasing the repulsion strength. These observations are in qualitative agreement with the experimental results.

2. Theoretical Basis

Previously, it was shown that self-assembling of colloid spheres trapped at a water surface is governed by attraction forces due to capillary effects and the repulsion forces due to electrostatic dipole−dipole interaction between spheres. We have taken a similar approach to our simulations. In order to construct a model of collective behavior, the interaction between a pair of spheres, floating on an interface between a polar and a nonpolar fluid, was considered. Following the description by Nikolaides et al.[32] which is based on observations of small numbers of microspheres on an oil−water interface, we introduced an interaction potential representing the two types of forces. The minimum of the potential energy of this interaction leads to an equilibrium state for which the separation between the spheres is determined by the relative strength of the two balancing forces. The interaction potential is given as

$$U = \frac{F^2}{2\pi\gamma}\log\left(\frac{r}{r_0}\right) + \frac{p^2}{4\pi\varepsilon_0 r^3}\frac{2\varepsilon_{\text{air}}}{\varepsilon^2_{\text{water}}} \quad (1)$$

where

$$F \approx \frac{p^2}{16\pi\varepsilon_0 a_{\text{w}}^4}\frac{\varepsilon_{\text{air}}}{\varepsilon^2_{\text{water}}} \quad (2)$$

The first term in eq 1 is attributed to the capillary attraction and the second term to the dipolar repulsion. Here F is the force normal to the interface that distorts the interface, leading to an intersphere capillary attraction; γ is the interfacial energy; r_0 is the radius of the spheres; a_{w} is radius of the water-wetted area of the sphere; ε_{air}, $\varepsilon_{\text{water}}$, and ε_0 are dielectric constants of air, water, and vacuum, respectively; r is the center-to-center separation between the spheres; and p is the total electric dipole moment of the sphere which depends on the screening length and the surface charge density of the spheres. The minimum of the potential energy of this interaction gives rise to an equilibrium separation between spheres (r_{eq}) determined by their relative strengths. For the purposes of constructing a numerical model, the physical parameters were combined into two coefficients: A and R for the attractive and repulsive components, respectively. Equation 1 is then reduced to the form

$$U = A\log(r) + Rr^{-3} \quad (3)$$

The model was implemented using an iterative gradient-descent technique[43,44] searching for the spatial configuration of particles corresponding to the lowest-energy state of the whole assembly (see Appendix for a detailed description of the algorithm of the program). Minimization of potential is achieved by displacing each sphere at a time to reduce the total energy of the system. For each iteration step the interaction is computed for all pairs of particles in the system. The dynamic or hydrodynamic properties of the system are assumed to be negligible. Boundary conditions of the system model the external physical constraints of the system, such as the area of the water surface, and the size of the spheres themselves. These conditions were implemented simply by checking and correcting overlaps between spheres or overlaps between spheres and the boundaries. Certain ad-hoc modifications were also implemented to deal with side effects of approximations: the electrostatic interaction between the spheres was set to a constant value at very short-range to avoid artifacts caused by the inverse dependence of the repulsion. At long ranges, i.e., more than five sphere diameters, the attractive capillary interaction was set to zero to account for the fact that capillary effects occur only between spheres located at short distances from each other. For each iteration step the assembly of the spheres was visualized as a coordinate map, where each sphere was represented with a circle of the corresponding radius. Some of the maps were combined as animation movies in order to observe the evolution of the system. The maps of final positions of spheres were analyzed using fast Fourier transformation (FFT) to examine the degree of ordering. It was found that the close-packed assembled structures, where the equilibrium separation is less than the sphere diameter, would not yield ordered arrangements except for a very small (<40) numbers of spheres. For a larger numbers of spheres, a significant long-distance order, with clear domain boundaries, occurs when the repulsive contribution dominates. However, if the repulsion is too strong, the domain boundaries become less apparent, resulting in a glasslike structure with dominating short-range order. The best ordering has been achieved when a loose-packed ordered array is compressed by external forces, represented in the model by progressively moving boundaries, which compress a loose-packed array into close-packed array. This simulation process models the self-assembly of spheres assisted by two compression sliders as was implemented in the experimental method (see Figure 3).

3. Theoretical Calculations

The simulation routine is divided into three stages according to the running number of iterations. In the first initial stage, the system is driven only by the natural assembly. At the second stage, the resulting self-assembled structures are compressed by uniformly moving boundaries of the side walls toward the center until a closed-packed array of spheres is formed. Boundary wall movement has also been used in the experiment. Following the compression we allow our system to relax accounting for a number of additional iterations. In the code, the final steps within the first and the last stages were determined as iteration steps, during which there were no further recombinations in the system observed. In Figure 1 we show simulated maps of the geometrical positions of spheres for three simulation sets with different strengths of repulsion. Map a corresponds to the initial positions of 1000 spheres which are randomly distributed within the defined area. Maps b−d correspond to the results of assembly at different

(42) Pergamenshchik, V. M. *Phys. Rev. E* **2009**, *79*, 011407.

(43) Avriel, M. *Nonlinear Programming: Analysis and Methods*; Dover Publishing: Mineola, NY, 2003.

(44) Snyman, J. A. *Introduction to Basic Optimization Theory and Classical and New Gradient-Based Algorithms*; Springer Publishing: Berlin, 2005.

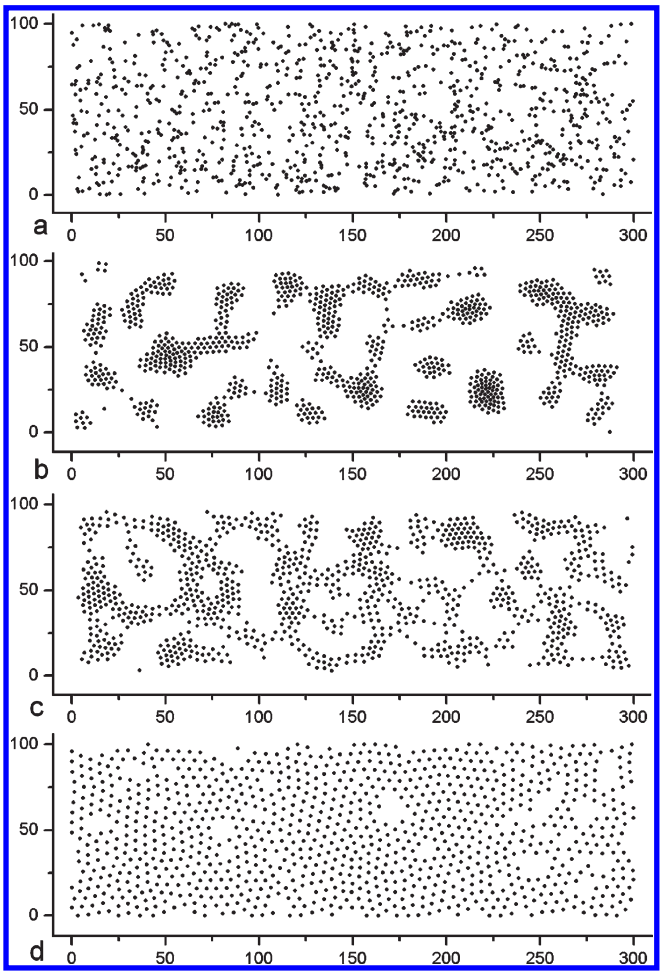

Figure 1. Simulated behavior of a large ensemble of interacting spheres with different strengths of repulsion. The maps of geometrical positions of spheres show (a) initial stage where the ensemble of 1000 spheres is randomly distributed within the fixed area; (b−d) correspond to equilibrium state of natural assembly at different repulsion-to-attraction (R/A) ratio (coefficient of attraction is fixed), from (b) to (d): R/A = 27, 31, and 63, respectively.

repulsion-to-attraction (R/A) ratios, where the coefficient of attraction A is fixed. Here the ratio R/A is 27, 31, and 63 in (b) to (d), respectively, and each map shows the specific self-assembled structure with different spacing between spheres. As can be seen from the simulated maps, when the self-assembly is not constrained by the boundaries at the same surface concentration of spheres, the structuring is governed entirely by the short-range interactions leading to the formation of localized clusters (Figure 1b). As the repulsion coefficient is increased, the sizes of the clusters are increased and occupy more of the area. Eventually, the clusters start interacting with each other,[42] leading to a formation of a cluster network (Figure 1c). Further increase of the repulsion coefficient leads to a filling of the voids (Figure 1d) until all empty areas are fully covered. In the latter cases, once the clusters are overlapped, the interaction between the spheres is affected not only by the neighboring units but also by the long-range contributions from the entire pattern. Similar structuring effects can be also achieved by varying concentration of the spheres, as was previously reported by Ruiz-Garca.[37] The degree of ordering, as can be seen qualitatively from the simulated maps, is increased as the spheres fill the whole available space, and the long-range interaction is achieved. Figure 2 shows the results of simulations after the second and final stages of assembly when the

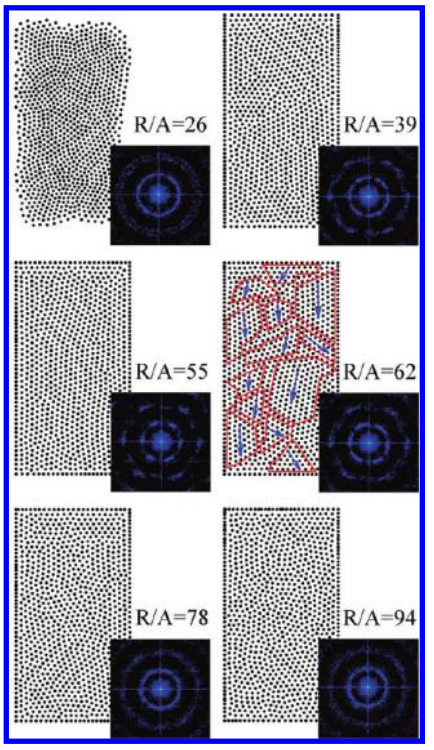

Figure 2. Simulated maps of the final geometrical positions of interacting spheres at different repulsion-to-attraction (R/A) ratios, achieved after natural assembly, compression, and further relaxation. Repulsive dipolar forces tend to form a more ordered array when the interaction strength between the spheres increases, until some point where it starts to go back again to a disordered system. The case of the best ordering was determined using FFT images (inset) and corresponds to R/A = 55.

boundaries are moved to reduce the available spatial area. The final positions of interacting spheres are shown for different repulsion-to-attraction (R/A) ratios. The simulated set of images reveals that at different strengths of repulsion the degree of ordering is different. As described below, the repulsive dipolar forces tend to form more ordered arrays when the interaction strength between the spheres is increased. However, at a certain R/A ratio, which we identify as a "transition" state, the directionality of lattice axes is lost, and the system goes back into a disordered state (R/A = 62). Similar reentrant order−disorder transitions were previously observed for ionic colloidal silica and polymer latex dispersions by varying particle charge density.[20−22] Our simulations showed that a particular attribute of the order−disorder transition in the case of 2D interactive particles is the formation of domains with a well-defined short-range order. The domains are separated by boundaries of dislocations. The orientation of lattice axes varies between different domains. When the repulsion force due to the long-range dipole interaction is further increased (Figure 2, $R/A > 78$), the boundaries become less defined, leading to a more glasslike structure. In order to quantify the results of ordering, we performed Fourier transform analysis of the spatial configurations. The insets of Figure 2 show the corresponding 2D fast Fourier transform (FFT) patterns. Each presented pattern shows a different degree of ordering corresponding to a different strength of repulsion. For R/A = 55 the simulated array was found to have the most ordered configuration of a spheres. The corresponding 2D FFT image of the array revealed a well-defined hexagonal diffraction pattern. This result follows the case (R/A = 39) of a domain structure with well-defined boundaries and large dimensions. On the basis of

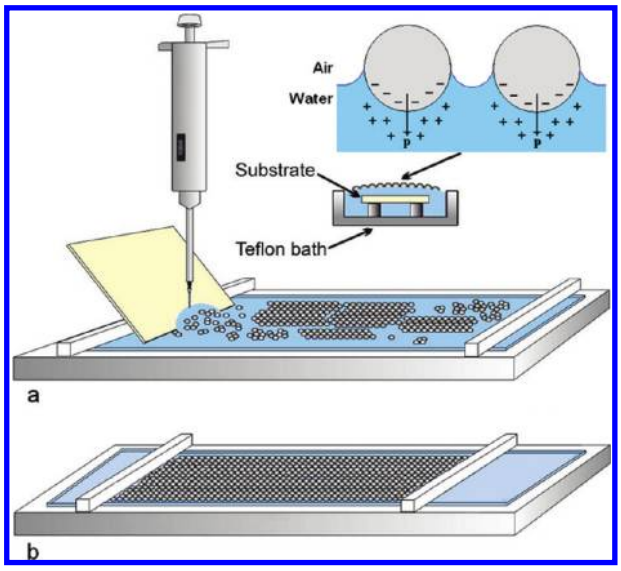

Figure 3. Experimental setup: (a) introducing the spheres onto the water surface and (b) compression of assembled structures into a confined monolayer. Assembled and compressed monolayers were deposited onto substrate located under water surface (as shown on the inset) by reducing the level of water. Inset: position of the substrate in the bath and a sketch of the charge distribution on spheres when submerged in water. Vector p demonstrates the polarization effect at the interface.[34]

the results of simulations, it was proposed that by varying the ratio between the attraction and repulsion coefficient, we could improve the self-assembling order to achieve larger domains with the ideal HCP lattice.

4. Materials and Methods

The experimental setup and methods used in this work have been described in detail in our previous publication.[34] The nanosphere solutions (Duke Scientific Corp.) are normally available as deionized water suspensions of hydrophilic polystyrene carboxylate-modified reagent microspheres. The surface of the spheres is terminated by reactive carboxyl groups which have Na^+ ions. When submerged in water, the surface cations are partly dissociated. The density of the surface carboxyl group, or "parking area", is normally varied and depends on the average size of the spheres. In our experiments we used two types of spheres, 390 and 780 nm with the corresponding "parking areas" of 46 and 51 $Å^2$/group, respectively. The spheres were purchased as "surfactant-free", so no special treatment was required to remove the surfactant from the colloids.[40] As described previously,[34] the experiments were performed at room temperature using deionized water with resistivity of 18 $M\Omega \cdot cm^2$. The self-assembly of nanospheres was carried out in a standard Langmuir−Blodgett trough with Teflon sliders (see Figure 3). Generally, we distinguish four main stages in the self-assembly of nanospheres: (i) dispensing of the spheres onto water surface; (ii) self-assembly process; (iii) compressing of the self-assembled areas into confined regions using Teflon sliders; and (iv) deposition of the compressed monolayer onto a substrate. Here we focus on the second and the third stages of the process. At the stage of self-assembly, when the surface concentration of spheres is high enough (in our case it is 60−80 μL of solution per 12−16 cm^2 of surface area), the formation of monolayer can be seen visually as diffraction of light reflected from the monolayer of spheres. Confinement by the trough boundaries leads to partial coverage of the water surface by the monolayer, even without the use of sliders. When the spheres are further compressed by the sliders, the dynamics of the monolayer depends on the electrochemical environment of the sphere−water interface. In order to control the repulsion-to-attraction ratio between spheres, we tuned the strength of repulsion. The strength of repulsion is readily manipulated by changing the chemistry of water solution. When the salt ions are added in an electrolyte solution, the repulsive forces between spheres are screened. On the other hand, the repulsive interaction between spheres becomes larger when a water solution is deionized. The chemical composition of the water in our experiments was modified by changing the salt concentration (NaCl) or pH factor (H_2SO_4). Two different reagents at different concentrations have been used in order to provide different rate of tuning strength. For instance, the use of NaCl is more efficient in our case, since by adding of Na^+ ions to water, we also change the effective surface charge density of sphere. At the same time, the use of acid (H_2SO_4) only increases the effect of electric screening of spheres in water. The assembled close-packed monolayers are then deposited (transferred) onto glass substrates for further microscopy and diffraction analysis.

5. Experimental Results and Discussion

To analyze the ordering characteristics of monolayers self-assembled at different electrochemical conditions, we employed scanning electron microscopy (SEM) imaging and laser diffraction. The latter has been used for analysis of the ordering of monolayers with large-area ordered domains. Here a continuous wave HeCd laser was used as the source of radiation with a wavelength $\lambda = 325$ nm and a spot size of 3 mm. The SEM images were taken at several different points across each sample in order to confirm the reproducibility of the domain structure through the whole area of the monolayer. In Figure 4 we show the set of characteristic SEM images and the corresponding FFT plots (insets) acquired for monolayers of 780 nm polystyrene spheres self-assembled at different pH factors of the water solution in the trough. As can be seen from Figure 4, increasing the pH factor leads to an increase in the domain size. We speculate that the electrostatic repulsion strength of spheres is modified with a reduced screening. The demonstrated interval of pH allows tuning of repulsion strength within the range that corresponds to the transition from a quasi-disordered array to macroscopically ordered monolayer. The experimental observations are in qualitative agreement with the simulation results where the increase of the repulsion strength leads to the increase in the ordering (compare the FFT results for $R/A = 26$ and $R/A = 55$ in Figure 2). The monolayer that demonstrates optimal ordering (pH = 5.3, Figure 4d) has been analyzed using laser diffraction to verify the ordering on a macroscopic length scale. The first-order hexagonal Bragg peaks indicate a uniform lattice of the spheres over the area exceeding that of the laser spot (~3 mm). It should be noted that the simulation results also predict the increased order and formation of the domain structure when the ratio R/A is increased (see Figure 2, $R/A = 39$). The simulation also predicted that further increase of the repulsion have to led to a configuration where the ordering is optimal ($\sim R/A = 55$). The following increase of the ratio R/A led to glasslike structures with reduced order. In the experiments with 780 nm spheres it was difficult to verify the latter stage as the maximum pH factor (5.3) we could achieve was that for the neutral water solution with added new "off-shelf" solution of microspheres. However, for older solutions, which typically tend to assemble into smaller domain structures, it was found that in many cases the increase of pH first increased the domain size and then leads to a reduction. These results are not demonstrated as it is difficult to quantify the degree of aging for the old solutions. Once opened, the sphere suspension is normally exposed to contamination and is likely to change its electrochemical properties within a certain period of

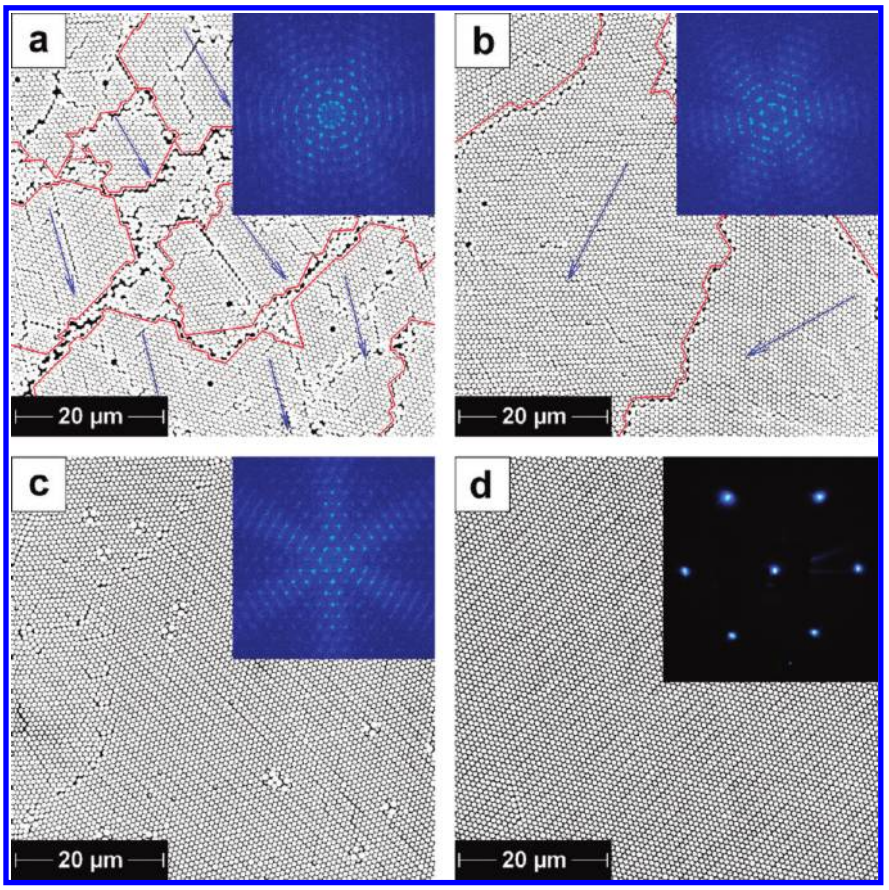

Figure 4. Characteristic SEM and the corresponding FFT images (insets) taken from monolayers of 780 nm size polystyrene spheres self-assembled in water of different pH. From left to right: pH = 2.3, 3.3, 4.5, and 5.3. Blue arrows indicate the direction of the principal axes within the domains. Red marked areas demonstrate the boundaries of ordered domains. The sample shown in (d) for pH = 5.3 has been analyzed with blue-laser diffraction (λ = 325 nm). The laser spot size (~3 mm) covers approximately the whole area of the chosen ordered domain. The diffraction image recorded in reflection shows well-defined hexagonal structure with minimal (< 1%) broadening of the peaks.

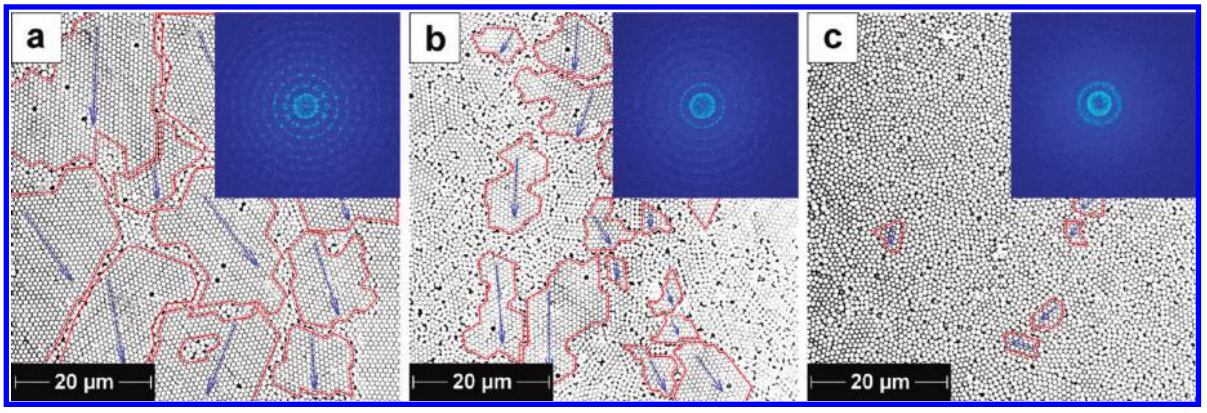

Figure 5. SEM and corresponding FFT images (insets) from monolayers of 780 nm size polystyrene spheres self-assembled at different salt concentrations C_s in water. The transition from quasi-disordered array to absolutely disordered system is presented from left to right for C_s = 0.03%, 0.22%, and 1.11%. Red marked areas show the size of single ordered domains.

time (typically ~1−3 months). It was also found that fresh suspensions of spheres with parking areas that are significantly larger than 50 Å^2/group, and hence having reduced surface charge density (e.g., 120 nm spheres, parking area 112 Å^2/group) showed a tendency to assemble instantly into tightly bound clusters of microscopic domains (< 5 μm) ones they suspended on the water surface, even without compression. These tightly bounded self-assembled regions cannot be modified by sliders. Because of weak electrostatic repulsion, these spheres have a lack of mobility which allows to reassemble into larger domains. These spheres form closed-packed rigid monolayer which tends to "crack" into smaller formations once the monolayer is disturbed by movements of the water or sliders. A similar effect was observed when attempting to assemble carboxyl nanospheres that were 390 nm in diameter with a parking area of 102 Å^2/group. On the other hand, the spheres that have a parking area significantly smaller than 50 Å^2/group, (i.e., 8 Å^2/group for 960 nm spheres) and hence significantly increased surface charge density show an opposite behavior. In this case the electrostatic repulsion is much greater than the attractive capillary force, and it is difficult to achieve

close-packed structure even with the compression by the sliders. These spheres have a tendency to "spread" or "flow", avoiding ordered formations. This is in contrast to the sphere solutions investigated here. It can be visually observed that the self-assembled monolayer is rather elastic and can easily increase its size if the confinement by the sliders is loosened up. We interpret this again as an increased repulsion due to the surface charge, which allows the spheres to increase the average separation between each other thus lead to an increase of the whole self-assembled region. Figure 5 shows the set of 60 × 60 μm^2 SEM images with the corresponding FFT images (insets) from monolayers of 780 nm size polystyrene spheres self-assembled at different salt concentrations dissolved in water (C_s). As described below, the increase in the concentration of Na^+ ions in the water in this case has an opposite effect. A large concentration of Na^+ ions reduces the dissemination of charge from the spheres and hence reduces the repulsion. Within the shown interval of C_s we can see that the domains of ordered regions are reduced and then nearly completely lost. (The interpretation of the boundaries in the case of C_s = 1.1% is ambiguous as there are no well-defined areas with well-defined lattices.) This indicates that the long-range correlation is reduced approaching the nearly disordered case for the larger concentration of salt. This is correlated with the simulation results shown in Figure 2 for R/A = 26, where the self-assembly has only short-order correlation and no domain structure. The FFT images (inset in Figure 5) support the loss of order in this case by showing nearly diffused scattering with only first three "rings" of intensity. It is interesting to note that reduction of the domain size is also accompanied by the increase of defects (voids, dislocations), which can be attributed to the loss of order. However, we believe that the defects themselves are not the reason for the lost correlation. It is often observed that although such defects affect the local order, on a larger scale, the domains and the lattice tend to preserve the structure. In Figure 6 we summarize experimentally determined average domain sizes in monolayers of 780 nm spheres as a function of pH factor (a) and salt concentration (b). The average size is estimated by measuring lateral dimensions of ~20 domains imaged by SEM from different areas of the film. The identical set of pH experiments has been performed with 390 nm spheres. As mentioned below, these spheres have a slightly lower value of the "parking area" (46 $Å^2$/group), which corresponds to a greater effective surface charge and hence to a stronger repulsion between the spheres. However, given the significant difference in size of the spheres, the variation of the domains is significantly different. Thus, in the considered range of pH values, the size of the domains is greater than the maximum field view of the SEM image for which the

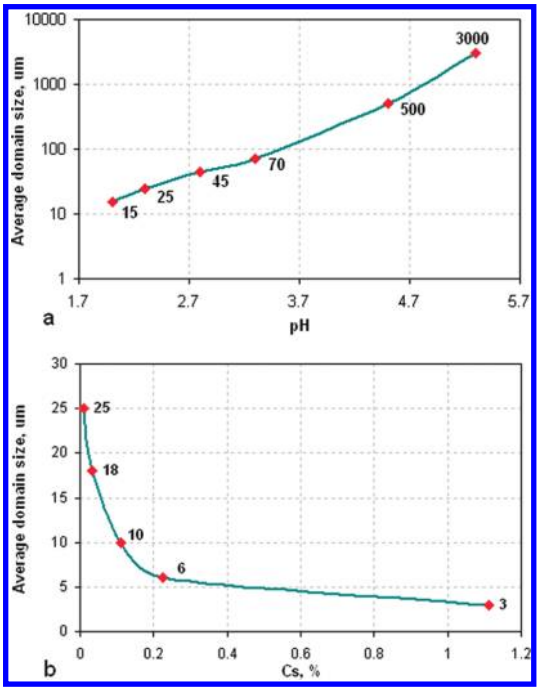

Figure 6. Average domain size in self-assembled monolayers of 780 nm size polystyrene spheres as a function of pH factor of water (a) and as a function of salt concentration (b). The size of domains at pH = 5.5 (a) is equal to or larger than the laser spot size (3 mm in diameter).

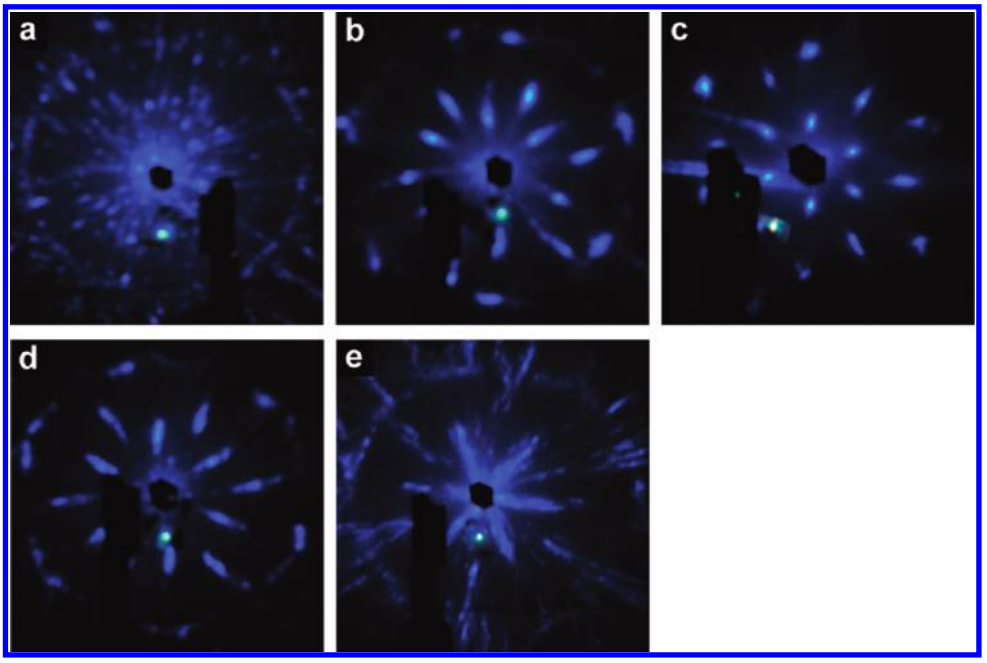

Figure 7. Characteristic blue laser (λ = 325 nm) diffraction patterns recorded in reflection from monolayers of 390 nm spheres self-assembled at different pH factor of water. From left to right: pH = 2.8, 3.7, 4.1, 4.9, and 5.5. The size of the laser spot is ~3 mm.

individual spheres can be resolved (so that FFT could be applied). Using optical microscopy, we have observed that as in the case of 780 nm spheres increasing the pH value in the bath has led again to variation of the domain size. In order to analyze the ordering characteristics, we have used laser diffraction. Figure 7 shows the set of laser diffraction patterns (taken in reflection) from monolayers assembled at different pH values. In Figure 7a the diffraction pattern is nearly defused, indicating a domain's size that is significantly less than the laser spot size. At pH of 3.7 (Figure 7b), the diffraction structure improves, showing a distorted hexagonal pattern. At pH = 4.1 (Figure 7c), the pattern at its best quality showing several orders of hexagonal peaks. For this pH value, the maximum size of the domains is achieved that exceed the size of the laser spot. The average size of the domains was found around 25 mm^2 in this case. Further increase of pH, Figure 7d,e leads first to a distortion of the hexagonal structure, most likely originating from partial reduction of the domain size, and then to a complete loss of the pattern. It should be noted that scattering is in the last case is not defuse (such as in the case of Figure 7a) but shows a certain hexagonal structure with the first-order peaks "spread" along the principal directions. A direct analogy with FFT images (in simulation) is not achieved because the scattering from the spheres is more complex than just a Fourier image from a pattern of dots. However, we speculate that in this case the long-range order may still be preserved, so the domain size is not varied, but the short-range order is affected. The latter can be due to defects during transfer of the monolayer to the substrate. Because of the increased separation between spheres, they become more mobile and when transferred to the substrate can move due to interaction with the substrate. Although the long-range order is maintained, the local correlations are affected. Compared with the results produced for 780 nm spheres for the range of pH in this case, we see that there is an optimum pH for which the ordering characteristics and the domain size are optimal. It should be noted that in both cases the optimal ordering and the size of the domains can be further improved by providing additional effects, such as mechanical vibration of the trough. In practice, this allows to increase the domain size up to 100 mm^2 and higher. Such effects are more complicated to simulate and are not described here.

6. Conclusions

In this work we have experimentally demonstrated that interaction forces, responsible for structural ordering, are the cause of macroscopic ordering for close-packed monolayers of polystyrene nanospheres. We have applied SEM imaging, FFT analysis, and laser diffraction to characterize the ordering parameters and their evolution in monolayers self-assembled at different electrochemical conditions. We have applied a numerical model that determines the geometrical configurations of interacting spheres according to the minima of the interaction potential. We speculate that there is a defined state of the potential energy when the order parameter is maximal. The simulations reproduce some qualitative agreement with the trend observed in the experiment. According to the experiment, macroscopic ordering over an area of 25 mm^2 is achieved using polystyrene spheres with correct surface chemistry. The possibility to control ordering on area up to macroscopic sizes by tuning the repulsion−attraction balance is simple for implementation, and self-assembled close-packed monolayer can be transferred onto almost any substrate. These self-assembled monolayers can be conveniently used as templates for lithographic applications. The described approach is technologically very attractive, since maintaining long-range order while achieving nanoscale resolution over macroscopic length scales is still a significant challenge for many conventional fabrication techniques. Thus, large hexagonal arrays of almost any materials can be produced with an improved order over macroscopic length scales which provides a route for creating technologically important patterned materials.

Acknowledgment. The authors gratefully acknowledge the financial support of the University of Exeter Research Fund in this work. The authors also would like to thank Dr. Peter Petrov for the valuable discussions on this work.

Appendix. Algorithm of the Simulation Routine

1. Positioning the Particles within the Area of the Bath. The coordinates of the sphere centers are randomly allocated using the generic pseudorandom generator. If any new center happens to be within radius of the center of another particle, it is moved away in a random orientation over the distance exceeding it. The same condition is forced for the boundaries of the bath.

2. Evaluation of the Potential Gradient. For each sphere, the potential U (eq 3) and its gradient ∇U are evaluated. For separations $\mathbf{r}$ less than the one diameter and more than 5 diameters of a sphere the variation in potential is ignored.

3. Moving the Sphere to the Position with the Lower Potential Value. For each particle the new iterative displacement is evaluated using the spatial derivative of the current potential.

$$\mathbf{r}_{n+1} = \mathbf{r}_n - \nabla U\beta$$

where $\mathbf{r}_n$ is the current position of the sphere, $\mathbf{r}_{n+1}$ is the new position of the sphere, and β is a fixed constant $\ll 1$. β defines the size of an iterative displacement. Larger values produce larger displacements and a "faster" approach to an equilibrium state. If β is too large, the convergence may not be achieved if the system is too far from the equilibrium. (In our simulations β was fixed to 0.0001; this produced a steady and a uniform descent.)

4. Corrections for Boundary Conditions. Similar to the positioning of the spheres in step 1, if at a particular displacement the sphere overlaps with another sphere or a boundary of the trough, it is forced to be positioned at the closest point on the boundary. This condition is applied also in the case when simulating movement of the sliders.

5. End of Iterations. When a variation in potential is reduced below a given threshold number or the total number of iterations exceeds a limiting number, the program is stopped and the final positions of all spheres are printed out in a file.